Cancer Research

N^6-Methyladenosine Modulates Nonsense-Mediated mRNA Decay in Human Glioblastoma

Fuxi Li[1,2], Yang Yi[3], Yanyan Miao[4], Wenyong Long[5], Teng Long[1,2], Siyun Chen[1,2], Weisheng Cheng[2], Changye Zou[6], Yueyuan Zheng[4], Xingui Wu[2], Junjun Ding[2], Kaiyu Zhu[4], Delin Chen[1,2], Qiongcong Xu[7], Jinkai Wang[1,2], Qing Liu[5], Feng Zhi[8], Jian Ren[4], Qi Cao[3,9], and Wei Zhao[1,2]

Abstract

The N^6-methyladenosine (m^{6}A) modification influences various mRNA metabolic events and tumorigenesis, however, its functions in nonsense-mediated mRNA decay (NMD) and whether NMD detects induced carcinogenesis pathways remain undefined. Here, we showed that the m^{6}A methyltransferase METTL3 sustained its oncogenic role by modulating NMD of splicing factors and alternative splicing isoform switches in glioblastoma (GBM). Methylated RNA immunoprecipitation-seq (MeRIP-seq) analyses showed that m^{6}A modification peaks were enriched at metabolic pathway–related transcripts in glioma stem cells (GSC) compared with neural progenitor cells. In addition, the clinical aggressiveness of malignant gliomas was associated with elevated expression of METTL3. Furthermore, silencing *METTL3* or overexpressing dominant-negative mutant METTL3 suppressed the growth and self-renewal of GSCs. Integrated transcriptome and MeRIP-seq analyses revealed that downregulating the expression of METTL3 decreased m^{6}A modification levels of serine- and arginine-rich splicing factors (*SRSF*), which led to YTHDC1-dependent NMD of *SRSF* transcripts and decreased SRSF protein expression. Reduced expression of SRSFs led to larger changes in alternative splicing isoform switches. Importantly, the phenotypes mediated by METTL3 deficiency could be rescued by downregulating *BCL-X* or *NCOR2* isoforms. Overall, these results establish a novel function of m^{6}A in modulating NMD and uncover the mechanism by which METTL3 promotes GBM tumor growth and progression.

Significance: These findings establish the oncogenic role of m^{6}A writer METTL3 in glioblastoma stem cells.

Introduction

Nonsense-mediated mRNA decay (NMD) contributes to mRNA surveillance pathways that affect a broad spectrum of cellular functions and maintain homeostasis. Although the primary function of NMD in reducing errors in gene expression by eliminating mRNA transcripts that contain premature termination codons (PTC) is well known, the mechanisms of target mRNA selection for NMD are still not well understood.

RNA methylation is a reversible modification of mRNA and has been linked to many types of cancer. N^6-Methyladenosine (m^{6}A) represents the most abundant methylation modification of mRNAs in eukaryotes (1–3), and it regulates almost every aspect of mRNA metabolism, including RNA processing (4, 5), transport from the nucleus to cytoplasm (6, 7), translation (8, 9), and decay (10, 11). The m^{6}A methylation marks on mRNA are dynamically regulated in mammals through the methyltransferase complex, composed of the catalytic subunit METTL3, and demethylases (e.g., FTO and ALKBH5; refs. 7, 11–13) and are detected by "m^{6}A readers." YTH domain–containing proteins, including YTHDF1-3, YTHDC1, and YTHDC2, act directly as "m^{6}A readers" and can interact with distinct subsets of m^{6}A sites to produce different effects on RNA processing (9, 10, 14–16). The function of m^{6}A RNA methylation is highly variable and context-dependent, and its underlying mechanisms in the recognition of NMD targets are not well understood.

Recent studies have revealed that m^{6}A methylation of mRNA results in diverse regulatory functions in cancer initiation and

[1]RNA Biomedical Institute, Sun Yat-sen Memorial Hospital, Sun Yat-sen University, Guangzhou, China. [2]Key Laboratory of Stem Cells and Tissue Engineering, Sun Yat-sen University, Ministry of Education, Guangzhou, China. [3]Department of Urology, Northwestern University Feinberg School of Medicine, Chicago, Illinois. [4]State Key Laboratory of Oncology in South China, Cancer Center, Collaborative Innovation Center for Cancer Medicine, School of Life Sciences, Sun Yat-sen University, Guangzhou, China. [5]Neurosurgery Department, Xiangya Hospital, Central South University, Changsha, Hunan, China. [6]Musculoskeletal Oncology Center, The First Affiliated Hospital of Sun Yat-sen University, Guangzhou, China. [7]Department of Pancreatobiliary Surgery, The First Affiliated Hospital of Sun Yat-sen University, Guangzhou, China. [8]Department of Neurosurgery, The First People's Hospital of Changzhou, Changzhou, Jiangsu, China. [9]Robert H. Lurie Comprehensive Cancer Center, Northwestern University Feinberg School of Medicine, Chicago, Illinois.

Note: Supplementary data for this article are available at Cancer Research Online (http://cancerres.aacrjournals.org/).

F. Li, Y. Yi, and Y. Miao contributed equally to this article.

Corresponding Authors: Wei Zhao, Zhongshan School of Medicine, Sun Yat-sen University, Guangzhou 510080, China. Phone: 86-13-9289-76506; Fax: 86-20-87330567; E-mail: zhaowei23@mail.sysu.edu.cn; and Qi Cao, Northwestern University, 303 E Chicago Avenue, TARRY 16-759, Chicago, IL 60611. Phone: 312-503-5990; E-mail: qi.cao@northwestern.edu

Cancer Res 2019;79:5785–98

doi: 10.1158/0008-5472.CAN-18-2868

progression. In addition, dysregulated m^6A methylation is closely related to various types of cancers. It has been reported that the m^6A methyltransferase METTL3 is required for the growth, survival, and invasion of cancer cells (17–19). The m^6A demethylase FTO was found to play a critical oncogenic role in promoting acute myeloid leukemia (AML; ref. 20). Although evidence is emerging, linking m^6A modulators and tumorigenesis, it remains to be determined whether m^6A modifications on different regions of mRNA, recognized by distinct readers, will lead to different cell fates. METTL3 elevates m^6A methylation modification to promote glioma stem cells (GSC) stemness by enhancing *SOX2* stability in glioblastoma (GBM; ref. 21). Controversially, another research group found that knockdown (KD) of *METTL3* dramatically promoted GSC self-renewal and tumorigenesis (22). Moreover, ALKBH5, which decreases m^6A modification in GSCs, exerts an important tumorigenic role in the progression of GBM through regulation of FOXM1 expression (23). These findings have raised questions about whether m^6A methylation modifications that affect GBM progression are dependent on the RNA sequence and are dynamically regulated.

Here, we observed preferential distribution of m^6A peaks in GBM cells. Elevated METTL3 in clinical specimens correlated with higher grades of gliomas, increased tumor recurrence, and worse clinical outcomes. Moreover, we found that silencing of *METTL3* led to reduced aggressive and tumorigenic capabilities, as well as diminished GSC phenotypes in GBM cells. Methylated RNA immunoprecipitation-seq (MeRIP-seq) and RNA-seq analyses revealed that KD of *METTL3* led to downregulation of NMD-targeted splicing factor mRNA transcripts that was dependent on the m^6A reader YTHDC1. Importantly, splice alterations of targeted mRNAs were critical for tumor growth inhibition and suppression of stemness due to *METTL3* KD. Together, our study identifies m^6A methyltransferase METTL3 as a modulator of NMD to sustain malignancy in GBM.

Materials and Methods

Glioma specimens and brain tissue collection

Both GBM and normal brain tissue surgical specimens were collected in The First People's Hospital of Changzhou and Xiangya Hospital of Central South University, in accordance with institution-approved protocols. Written informed consent was obtained from each study participant after a thorough explanation of the procedure and its risk, in compliance with the Declaration of Helsinki. Collected specimens were further split into two parts for RNA extraction and protein isolation. If only a limited amount of specimens was obtained, only an RNA extraction assay was performed. Three freshly obtained specimens were specifically used for primary cell establishment (see section below). All specimens were examined by neuropathologists to verify tumor types and grades.

Cell culture and reagents

The human GBM cell lines of U251 and U87MG were provided as a gift from Dr. Jun Cui's laboratory at Sun Yat-sen University and were grown in Gibco DMEM containing 10% FBS (Gibco) at 37°C in a humidified atmosphere containing 5% CO_2.

For the culture of primary GBM cells, surgically removed GBM specimens were washed with and minced in sterile PBS. Next, a single-cell suspension was obtained by pressing the minced tissues through 40-μm cell strainers (Falcon). Dissociated cells were cultured in DMEM supplemented with 15% FBS (Gibco), 1 × B27 (Invitrogen), 20 ng/mL epidermal growth factor (CantonBIO), and 20 ng/mL FGF (CantonBIO) at 37°C in a humidified atmosphere containing 5% CO_2. All primary cells were passaged every 7 days.

Subcutaneous tumor model and intracranial GBM xenograft model

Five-week-old female Balb/c athymic nude mice were purchased from Model Animal Research Center of Nanjing University and housed in individually ventilated microisolator cages. Nude mice were divided into three groups of 6 mice each.

For subcutaneous tumor model, each mouse was injected subcutaneously in the right flank with 2×10^6 U87MG cells (*METTL3*-KD or control) in 100-μL PBS. Tumor sizes were determined with calipers every 5 days by measuring the length and width. Tumor volumes were calculated according to the following formula: volume (mm^3) = (length × width × width)/2. Fifty-eight days after the tumor cell injection, the mice were sacrificed and tumor xenografts were removed, weighted, fixed in formalin, and stored at 4°C.

For intracranial GBM Xenograft Model, each mouse was intracranially injected with 5×10^5 luciferase-transduced U87MG cells (*METTL3*-KD or control) in 10-μL PBS solution as described previously (24). Tumor growth was monitored by using a Xenogen IVIS Spectrum system (Caliper Life Sciences) weekly.

Animal experiments were approved by the Animal Care and Use Committee of Sun Yat-sen University.

Measurements of total m^6A mRNA levels

Total m^6A content was measured in 200-ng aliquots of total RNA extracted from *METTL3*-KD or scrambled, control U87MG, or U251 GBM cells using an m^6A RNA methylation quantification kit (EpiGentek), according to the manufacturer's instructions.

MeRIP-seq

Total RNA was isolated from *METTL3*-KD or scrambled control U87MG GBM cells, as mentioned above, and the mRNA was further separated using Dynabeads mRNA Purification Kit (Invitrogen, 61006). After fragmentation, using RNA fragmentation reagent (Invitrogen, AM8740), the obtained mRNA was immunoprecipitated with anti-m^6A antibody (Synaptic Systems, 202003), and then washed and eluted by competition with m^6A sodium salt (Sigma-Aldrich, M2780). Both input samples and immunoprecipitation (IP) eluates were used for preparing the sequencing libraries using NEBNext Ultra RNA Library Prep Kit for Illumina and submitted for sequencing using Illumina HiSeq 2500. Reads, mapping and m^6A peak calling, were performed as previously described (25). The m^6A peaks of sh*METTL3* U87MG cells were from the overlapped peaks of sh*METTL3*-1 and sh*METTL3*-2.

RNA immunoprecipitation-qPCR analysis

In YTHDC1 RNA immunoprecipitation (RIP)-qPCR experiments, U87MG cells were harvested and lysed in IP lysis buffer (150 mmol/L KCL, 0.5 mmol/L DTT, 5 mmol/L EDTA, 0.5% NP-40, 25 mmol/L Tris, pH 7.4). Each lysate was further divided into three groups for anti-YTHDC1, anti-IgG (negative control), and input (positive control). Either YTHDC1 antibody (Abcam) or IgG was added to each sample to enrich RNA-binding protein (RBP). Subsequently, the RBP of interest, together with the bound RNA, was collected using Dynabeads (Thermo Fisher Scientific).

After washing off unbound material, the RBP was digested by proteinase K, and the RNA bound to immunoprecipitated RBP was purified and reverse transcribed into cDNA. Then, qPCR assay was performed to measure the %Input of *SRSFs* mRNAs in each group. The primer sequences used for RIP-qPCR analysis were provided in Supplementary Table S2.

Statistical analysis

All analyses were performed using GraphPad Prism version 5.0 (GraphPad Software). The survival curves for combined expression of *METTL3* and splicing factors were plotted according to the Kaplan–Meier method, using PROGgene V2 software online (http://watson.compbio.iupui.edu/chirayu/proggene/). The association among the expression levels of *METTL3* and splicing factors was analyzed using Spearman rank correlation. Data were presented as the mean ± SD, and the significance levels of all tests were two-sided. The *P* value of less than 0.05 was considered statistically significant and marked as *; a *P* value less than 0.01 or 0.001 was marked as ** and ***, respectively.

Results

The m^{6}A methylome in GSCs is distinct from that of normal neural progenitor cells

Previous studies have suggested that GSCs are derived from mutated neural progenitor cells (NPC), which are critical for GBM tumorigenesis (26). Using MeRIP-seq data from GSE87515 (23) and GSE54365 (27), we first compared the m^{6}A peaks at each locus between GSCs and NPCs, respectively (Fig. 1A) and then divided the peaks into three categories comprising gene loci with m^{6}A peak enrichment in (i) both GSCs and NPCs; (ii) GSCs, or (iii) NPCs (denoted as "shared," "GSC," and "NPC," respectively; Fig. 1B; Supplementary Fig. S1A). We found that 9,627 loci in GSCs had elevated levels of m^{6}A modifications that were initially unmodified in NPCs (Fig. 1B). We further analyzed the signaling pathways of the three categories and found that loci with elevated levels of m^{6}A modifications were associated with metabolic pathways (Fig. 1C; Supplementary Fig. S1B). Specifically, the cancer metabolism–associated loci *TGFB2*, *TGFB3*, and *TEAD2* were highly enriched with m^{6}A modifications in GSCs (Fig. 1D).

The m^{6}A methyltransferase METTL3 is elevated in GBM clinical specimens

To determine the expression of m^{6}A modulators in GBM, we first queried the Repository for Molecular Brain Neoplasia Data (REMBRANDT) datasets. Compared with normal brain controls, GBM specimens displayed increased levels of *METTL3*, *METTL14*, *YTHDF1*, and *YTHDF2* (Supplementary Fig. S2A). To confirm these findings, we examined the mRNA expression of m^{6}A modulators in 36 GBM specimens from the First People's Hospital of Changzhou. *METTL3* and *YTHDF2* were markedly elevated in GBM patient samples as compared with normal brain tissues (Fig. 2A). Western blot analysis also showed higher METTL3 protein levels in GBMs compared with that in normal brain tissues (Supplementary Fig. S2B). Next, we examined METTL3 expression in a paraffin-embedded human glioma tissue array by IHC. As expected, there were remarkably more METTL3-positive cells in GBMs (grade 4) than in normal brain tissues or in lower grade gliomas (Fig. 2B). Intriguingly, significantly higher levels of METTL3 were found in recurrent tumors compared with paired, original tumors (Fig. 2C).

Next, we designed a screen based on a CRISPR/Cas9 library of sgRNAs to identify potential m^{6}A modulators regulating GBM cell proliferation and GSC sphere formation (Supplementary Table S1; Supplementary Fig. S2C). We transduced U87MG cells with 16 sgRNA lentiviral supernatants (one sgRNA per well), containing a puromycin selection cassette to eliminate uninfected cells. Infected cells were grown in a two-dimensional monolayer and three-dimensional Matrigel for 7 days. After three rounds of screening, we found that METTL3 and YTHDF2 were involved in the maintenance of GBM cell proliferation (Supplementary Fig. S2D) and sphere-forming capacity (Fig. 2D). Notably, high *METTL3* levels in GBMs predicted poorer patient survival [GBM patient data from REMBRANDT, GSE7696 (28), and GSE43378 (Fig. 2E; ref. 29)]. However, the expression of other modulators, except *YTHDF2*, did not significantly correlate with the time of GBM patient survival (Supplementary Fig. S2E). Collectively, METTL3 was upregulated in GBMs and may be critical for tumor growth.

The m^{6}A methylation catalytic domain of METTL3 is essential for its function in GBM

To test whether METTL3 was essential for GBM cell growth, we suppressed the expression of METTL3 in GBM cells through shRNA-expressing lentiviruses. Both sh*METTL3*-1 and sh*METTL3*-2 could downregulate METTL3 expression in GBM cells (Supplementary Fig. S3A and S3B). As expected, depletion of METTL3 also led to significantly reduced m^{6}A modification levels of mRNAs in both GBM cell lines (Supplementary Fig. S3C). Compared with cells expressing control shRNAs, both *METTL3*-KD GBM cell lines (U87MG and U251) showed significantly reduced cell proliferation (Fig. 3A). Similar results were also obtained in *METTL3*-KD primary GBM cells derived from 3 patients with GBM at Xiangya Hospital (Fig. 3A). Moreover, overexpression of the m^{6}A catalytic inactive mutant METTL3 acted in a dominant-negative manner to suppress cell growth and m^{6}A modification levels of mRNAs in U87MG and U251 cells (Fig. 3B; Supplementary Fig. S3D and S3E). Consistent with previous reports, *METTL3* KD increased the proportion of apoptotic cells in GBMs (Fig. 3C; Supplementary Fig. S3F). Furthermore, *METTL3* KD resulted in significantly decreased migration and invasiveness of GBM cells (Supplementary Fig. S3G and S3H). Conversely, overexpression of the METTL3 dominant-negative mutant in GBMs inhibited cell migration and invasion (Supplementary Fig. S3I). These data support an important role of the m^{6}A catalytic domain of METTL3 in controlling GBM cell growth, survival, and invasion *in vitro*.

We further investigated whether METTL3 inhibits the tumorigenic capacity of GBM cells *in vivo*. When U87MG cells, transduced with sh*METTL3* lentiviruses, were inoculated into nude mice, the cells produced much smaller xenograft tumors than cells expressing scrambled, control shRNAs (Supplementary Fig. S3J and S3K). Subsequently, the excised xenograft tumors were processed for IHC and terminal deoxynucleotidyl transferase–mediated dUTP nick end labeling assay (Supplementary Fig. S3L). Significantly reduced ratios of KI67-positive cells to apoptotic cells were observed in *METTL3* KD cell-derived tumors (Supplementary Fig. S3L).

Compared with the control shRNA, both sh*METTL3* sequences significantly decreased stem cell size (Supplementary Fig. S4A),

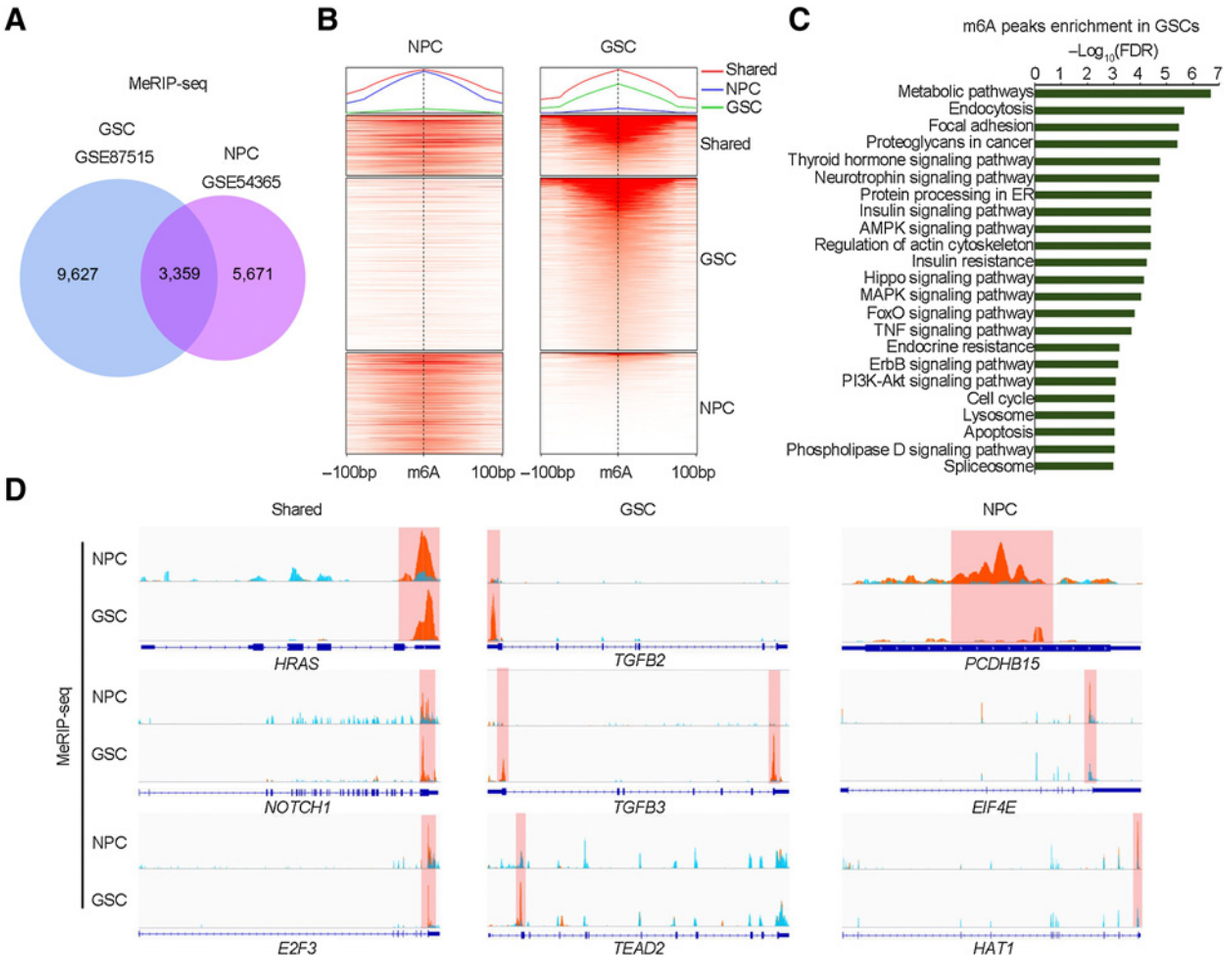

Figure 1.
The m^{6}A methylome in NPCs and GSCs. **A,** Venn diagrams of m^{6}A modification peaks between NPCs and GSCs. **B,** Heatmap and overlaps of m^{6}A MeRIP-seq signals for NPCs (GSE54365) and GSCs (GSE87515). The global m^{6}A modification status was arranged into three groups according to m^{6}A modification enrichment (enrichment score >1.5): shared (genes with m^{6}A modification in both GSCs and NPCs), GSC (genes with m^{6}A modification in GSCs but not in NPCs), and NPC (genes with m^{6}A modification in NPCs but not in GSCs). **C,** Kyoto Encyclopedia of Genes and Genomes analyses of genes with increased m^{6}A modifications in GSCs. **D,** The m^{6}A modification status of the represented genes from three groups.

number (Fig. 3D), and frequency (Fig. 3E) in GSC-derived tumor neurospheres. Whereas overexpression of WT METTL3 promoted U87MG and U251 neurosphere formation and stem cell frequency, the METTL3 mutant inhibited these phenotypes (Fig. 3F; Supplementary Fig. S4B and S4C). Moreover, sh*METTL3* decreased the CD133-positive populations in U251- and U87MG-derived neurospheres (Supplementary Fig. S4D). Compared with the mice injected with control U87MG spheroid-derived GSCs, those injected with shMETTL3 spheroid-derived GSCs displayed impaired tumor growth and a lower rate of tumor formation (Fig. 3G).

The m^{6}A modifications of splicing factor mRNAs are regulated by METTL3

To map m^{6}A modification sites and unveil potential METTL3 functions in GBM, we performed MeRIP-seq on U87MG cells with silenced *METTL3* (Supplementary Fig. S5A and S5B). Consistent with previous studies, we demonstrated that m^{6}A peaks in GBMs were enriched in the RGACH motif (R = G/A; H = A/C/U; Fig. 4A), and abundant in coding sequences (CDS) and untranslated regions (UTR) of mRNAs (Fig. 4B). Compared with the control GBMs, the m^{6}A peaks across entire gene bodies and 3′UTRs were markedly decreased in sh*METTL3* GBMs (Supplementary Fig. S5C). Furthermore, 6,444 genes with significantly decreased m^{6}A levels in sh*METTL3* GBMs were identified as potential m^{6}A-regulated genes (Fig. 4C). Moreover, carcinogenesis pathways were significantly enriched in these m^{6}A-regulated genes (Fig. 4D), suggesting a role for METTL3-mediated m^{6}A modifications in GBM tumorigenesis.

We further characterized the molecular signaling pathways regulated by METTL3 using RNA-seq (Fig. 4E; Supplementary Fig. S5D and S5E). Transcripts encoding apoptotic signaling pathways and glial cell differentiation genes were enriched in both *METTL3*-KD GBM cells (Fig. 4F and G). The upregulated expression of apoptotic and differentiation genes was confirmed by RT-qPCR (Fig. 4H). Interestingly, a large number of genes were

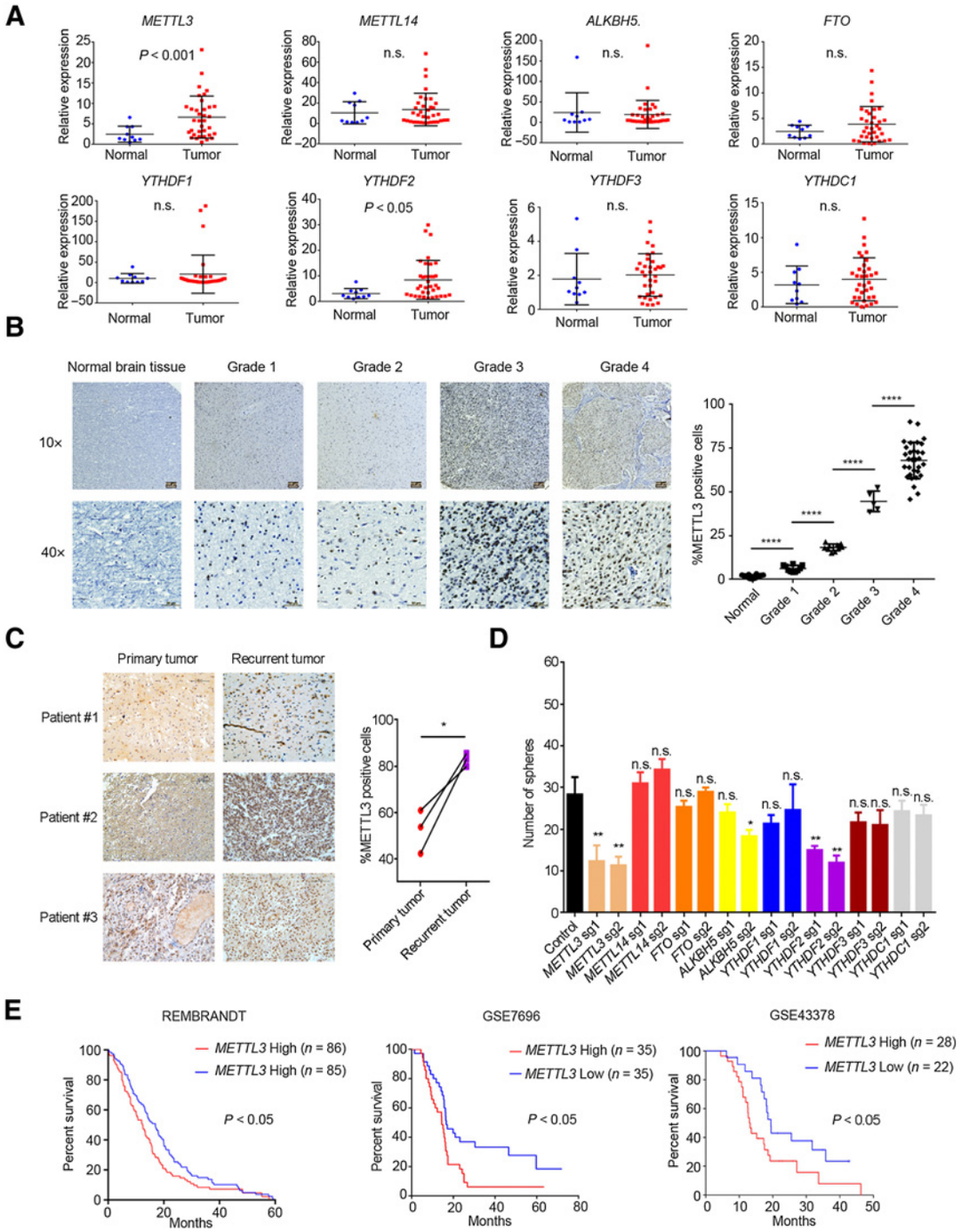

Figure 2.

Increased expression of METTL3 in GBM cells and in classical tumors. **A,** Expression of m^{6}A modulators was measured by qPCR in GBM specimens ($n = 35$) and compared with normal brain tissues ($n = 10$). **B,** IHC staining of METTL3 in patients with gliomas (grades 1–4) and comparison with normal brain tissue. The statistical results showed the proportion of METTL3-positive cells in each group. **C,** IHC staining of METTL3 in primary and recurrent GBM tumors from three patients with GBM. The statistical results showed the proportion of METTL3-positive cells in each group. **D,** The sphere-forming efficiency was plotted postinhibition of m^{6}A modulators using two different sgRNAs in U87MG cells. The number of spheres formed after 7 days were counted using ImageJ software. **E,** The association between *METTL3* expression in GBM and overall survival time of the selected patients was analyzed by Kaplan–Meier analysis. *, $P < 0.05$; **, $P < 0.01$; ****, $P < 0.0001$ is based on the Student *t* test. All results are from three independent experiments. Values are mean ± SD. n.s., no significant difference.

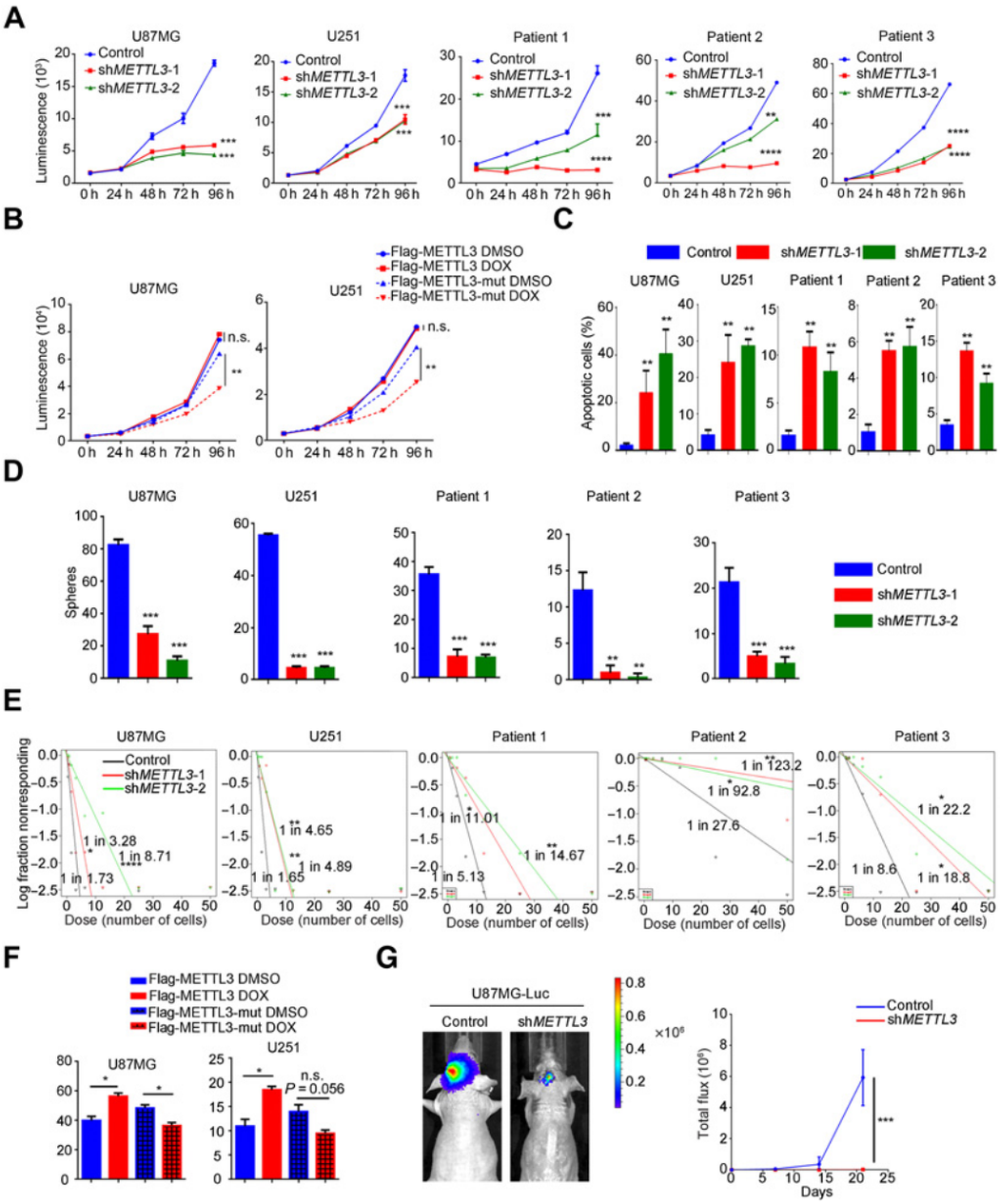

Figure 3.

Impairment of GBM proliferation and tumorigenicity by METTL3 inhibition. **A,** The cell viability tests of U87MG, U251, and primary GBM cells transduced with sh*METTL3* were performed using CellTiter-Glo. **B,** The cell viability tests of U87MG and U251 cells overexpressing wild-type (WT) METTL3 or METTL3 with a mutated catalytic domain (METTL3-MUT) were performed using CellTiter-Glo. **C,** The proportion of apoptotic cells in *METTL3*-KD and control GBM cells was evaluated by flow cytometry. The statistical results showed the proportion of Annexin V^+ PI^- cells, which indicate the amount of apoptotic cells in each group. **D,** Sphere-forming assay after *METTL3* silencing in U87MG cells compared with control cells. The number of spheres formed was counted after transferring spheres to stem cell culture conditions for 7 days. **E,** Limiting dilution assay of GSCs transduced with control shRNA or *METTL3* shRNAs. **F,** U87MG and U251 cells were transduced with flag-tagged WT METTL3 or METTL3 with a mutated catalytic domain (METTL3-mut). The number of spheres formed was counted after transferring spheres to stem cell culture condition for 7 days. Representative images of the spheres shown at ×10 magnification. Scale bar, 100 μm. **G,** Xenogen images of brain tumors in GSC-grafted nude mice ($n = 4$) transplanted with U87MG sphere cells that were transduced with control shRNA or *METTL3* shRNA. The scale bar for bioluminescence intensity is shown on the right. *, $P < 0.05$; **, $P < 0.01$; ***, $P < 0.001$; ****, $P < 0.0001$ is based on Student *t* test. Values are mean ± SD of three independent experiments. n.s., no significant difference.

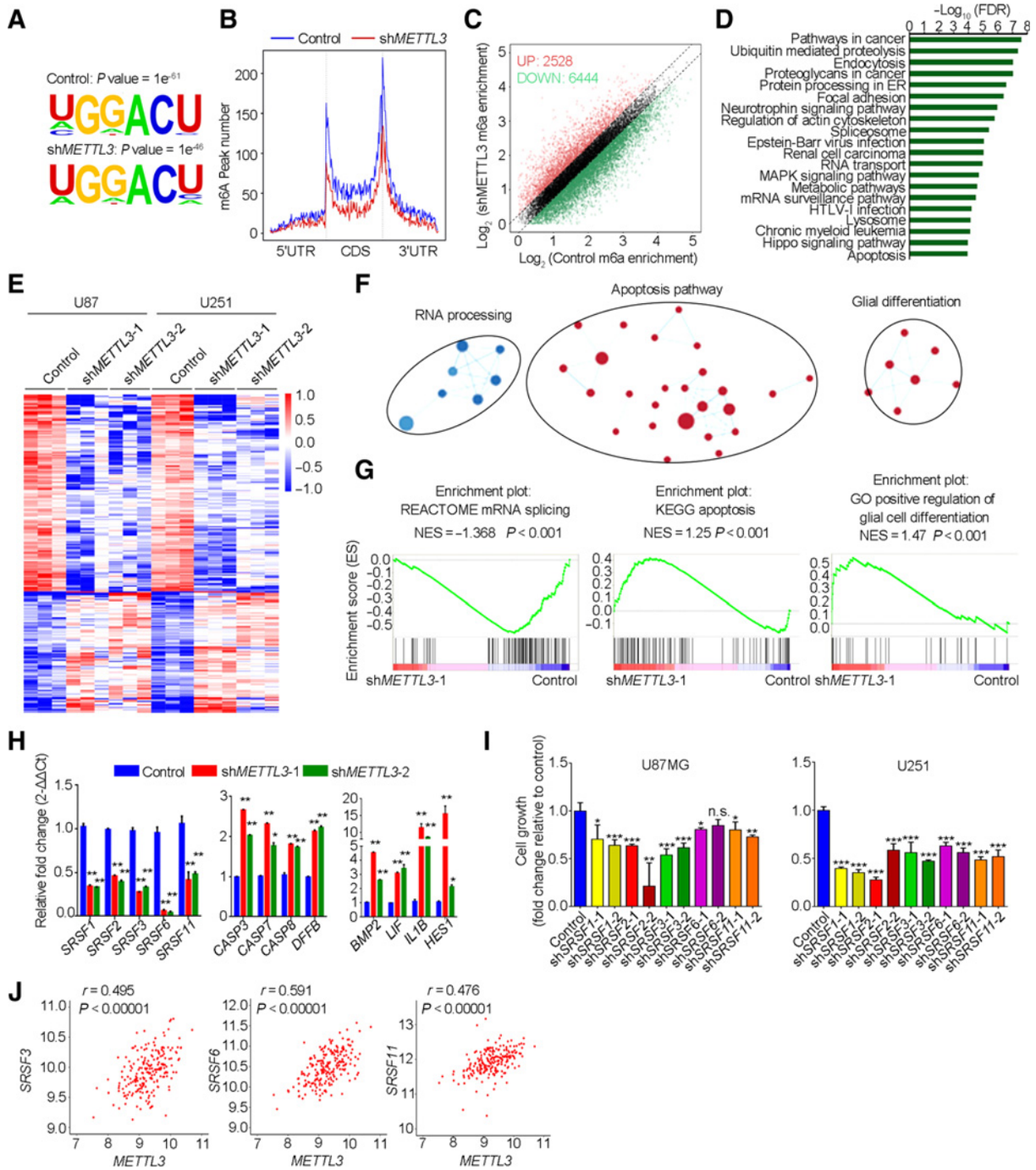

Figure 4.

Splicing factors are critical target genes of METTL3 in GBM. **A,** Motif analysis of m^{6}A modification peaks in control and *METTL3*-KD MeRIP-seq data. **B,** Distribution of m^{6}A modification peak reads across all mRNAs in control and *METTL3*-KD U87MG cells. **C,** Scatter plots showing the increased (red) and decreased (green) m^{6}A modification enrichment in mRNAs from control and *METTL3*-KD U87MG cells. **D,** Gene ontology analysis of mRNAs with decreased m^{6}A modification in *METTL3*-KD U87MG cells. **E,** Heatmap showing the mRNA expression changes in GBM cells depleted of METTL3. **F,** Gene ontology (GO) analyses of the genes differentially regulating genes between *METTL3*-KD and control cells. **G,** Gene set enrichment analysis enrichment plots of differentially regulated genes between *METTL3*-KD (sh*METTL3*-1) and control cells. Data of sh*METTL3*-2 drew same conclusion (data not shown). **H,** A qRT-PCR analysis. The mRNA levels were first normalized to the level of β-actin mRNA. The relative ratio (fold change) obtained in the presence of control shRNA was set to 1. **I,** U87MG or U251 cells transduced with indicated shRNAs were plated in a 96-well plate for 72 hours. Cell viability was assayed using CellTiter-Glo. **J,** Pearson correlation analysis of *METTL3* with *SRSF3, SRSF6*, or *SRSF11* based on REMBRANDT data. *, $P < 0.05$; **, $P < 0.01$; ***, $P < 0.001$ is based on Student *t* test. Values are mean ± SD of three independent experiments. n.s., no significant difference. KEGG, Kyoto Encyclopedia of Genes and Genomes.

also significantly downregulated in *METTL3*-KD cells. Gene ontology (GO) and gene set enrichment analysis analyses revealed that these downregulated genes were mainly involved in RNA processing and mRNA splicing (Fig. 4F and G). The downregulated expression of these splicing factors was also confirmed by RT-qPCR (Fig. 4H; Supplementary Fig. S5F). Next, we randomly selected several splicing factors regulated by METTL3 and found that KD of these genes impaired the proliferation of GBM cells (Fig. 4I; Supplementary Fig. S5G). Consistently, we found that *METTL3* expression positively correlated with splicing factors, especially *SRSF3*, *SRSF6*, and *SRSF11* (Fig. 4J; Supplementary Fig. S5H). GBM specimens displayed increased levels of *SRSF3/6/11* compared with normal brain controls (Supplementary Fig. S5I). Kaplan–Meier survival analysis revealed that patients with elevated expression of *METTL3* and *SRSF3/6/11* had shorter overall survival time (Supplementary Fig. S5J). Together, these results identify SRSFs as downstream targets regulated by METTL3, which are dysregulated in GBM.

The m^{6}A modification of splicing factor transcripts mediates mRNA selection for NMD

Expression of splicing factors is regulated via alternative splicing of the conserved regions to yield mRNAs, which are degraded by NMD. However, whether a significant proportion of splicing factor mRNA transcripts occur via reduced levels of m^{6}A modifications and are ultimately degraded by NMD is not known. NMD analyses using the *METTL3*-KD RNA-seq data revealed that the mRNA transcripts that undergo NMD were significantly enriched in genes associated with RNA splicing (Supplementary Fig. S6A). By comparing the m^{6}A modification of *SRSFs* in NPCs and GSCs, we found that m^{6}A modifications around start codon of splicing factor transcripts (e.g., *SRSFs*) were elevated (Fig. 5A; Supplementary Fig. S6B). The specific m^{6}A modification sites of the mRNAs of *SRSFs* were identified by miCLIP-seq analyses (Supplementary Fig. S6C; ref. 30). Importantly, on the basis of the markedly decreased m^{6}A modification peaks, premature termination (i.e., stop) codons (PTCs) in the mRNAs of *SRSFs* were generated via exon inclusion or skipping upon METTL3 depletion (Fig. 5B; Supplementary Fig. S6D and S6E). Therefore, these mRNAs with PTCs were predicted to be subject to NMD, and the predicted protein products were not physiologically relevant. A similar phenotype was also found in other splicing factors (Supplementary Fig. S6E). Silencing *METTL3* significantly reduced protein-coding mRNAs (mRNAs without PTCs) of *SRSFs* (Fig. 5C). In contrast, an inhibitory effect on mRNAs with PTCs was also observed upon overexpression of WT METTL3 (Fig. 5D). Moreover, protein-coding mRNAs of *SRSFs* were significantly decreased, upon overexpression of mutant METTL3 (Fig. 5E).

To investigate whether the mRNAs of *SRSFs* with PTCs were substrates for NMD, we analyzed steady-state levels of these mRNAs via inhibition of NMD. We used shRNA targeted at *UPF1* (Supplementary Fig. S6F), which is the central component of the NMD pathway. Treatment with shRNA against *UPF1* greatly increased the steady-state levels of the mRNAs with PTCs and total mRNAs of *SRSFs* (Fig. 5F). Similar increases in the levels of the mRNAs with PTCs were also observed after inhibition of NMD by treatment with cycloheximide (Fig. 5G). In addition, we found that the expression levels of *SRSFs* NMD variants were decreased in clinical GBM samples (Supplementary Fig. S6G).

The removal of m^{6}A modification around start codon of splicing factors is required for NMD in a YTHDC1-dependent manner

To analyze m^{6}A modification levels around start codon that modulate NMD signaling, we used a previously described (31) *in vitro* luciferase reporter systems (Fig. 6A). The reporter systems were derived from *SRSF6*, including the pre-mRNA sequence from transcription start site up to exon 3. The PTC in the intron 2 of *SRSF6* is maintained. In addition, we mutated the A with G to inactivate the m^{6}A modification–mediated exon inclusion. We observed that the *SRSF6*-Renilla–fused mRNA is m^{6}A modified (Supplementary Fig. S7A). Consistent with previous results, KD *METTL3* efficiently promoted the formation of the mRNA with PTC in the WT reporter, as indicated by reduced luciferase activity (Fig. 6B). However, no significant change of luciferase activity occurred in the reporter with the mutation in m^{6}A modification (Fig. 6B). Similarly, a lack of luciferase activity increase has also been observed with addition of the METTL3 mutant in GBM cells, compared with addition of the WT METTL3 (Fig. 6C). RT-qPCR analyses showed higher NMD RNA (RNA with PTC) levels and lower protein-coding mRNA (mRNA without PTC) levels in mutated *SRSF6* reporter compared with WT reporter, further suggesting that the m^{6}A modification is critical for inhibition of NMD (Supplementary Fig. S7B). Inhibition of NMD with sh*UPF1* greatly increased the Renilla-*SRSF6* NMD RNA and total mRNA of mutated reporter (Supplementary Fig. S7C). To further analyze the effects of m^{6}A modifications on NMD, a reporter was constructed consisting of exon 2, exon 3, and flanking intron sequences of *SRSF3* without m^{6}A modification site (Supplementary Fig. S7D). In contrast to the m^{6}A modification around start codon reporter system data, this reporter was greatly resistant to KD of *METTL3*-induced NMD (Supplementary Fig. S7E). Consistently, WT METTL3 cannot increase the luciferase activity of *SRSF3* minigene reporter contracts without m^{6}A modification site (Supplementary Fig. S7F).

Adenine base editing is a novel genome-editing approach to convert a target T•A to C•G without requiring homology-directed repair or introducing double-stranded DNA breaks (32). To generate m^{6}A site mutation in the *SRSFs* gene of interest in U87MG cells, we transduced the base editor construct and guide RNA targeting the *SRSF3* m^{6}A modification site around start codon (Fig. 6D). A total of 14 cell clones were obtained by limited dilution and Sanger sequencing indicated that nine carried the expected mutation (Fig. 6E). We next found that the NMD RNA of *SRSF3* significantly increased in m^{6}A-mutant U87MG cells compared with WT control (Fig. 6F). These results support that m^{6}A modifications around start codon mediate repression of NMD in GBM.

YTHDC1 has been reported as an m^{6}A modification reader that mediates mRNA splicing, and mutating either W377 or W428 to alanine completely disrupts its binding to m^{6}A RNA (15). KO of *YTHDC1* reduced sphere number substantially in METTL3 overexpression cells but not in control cells (Supplementary Fig. S7G). Overexpressing mutant YTHDC1 (m^{6}A binding activity loss) failed to enhance the sphere formation capacity of U87MG cells (Supplementary Fig. S7H), suggesting that YTHDC1 contributes to the GBM phenotype (e.g., sphere formation) dependently on its m^{6}A-binding activity. Moreover, RIP-qPCR assay results showed that YTHDC1 binds to *SRSF3*, *SRSF6*, and *SRSF11* mRNA when compared with negative control (Fig. 6G; Supplementary Fig. S7I). In addition, by analyzing PAR-CLIP-seq data from

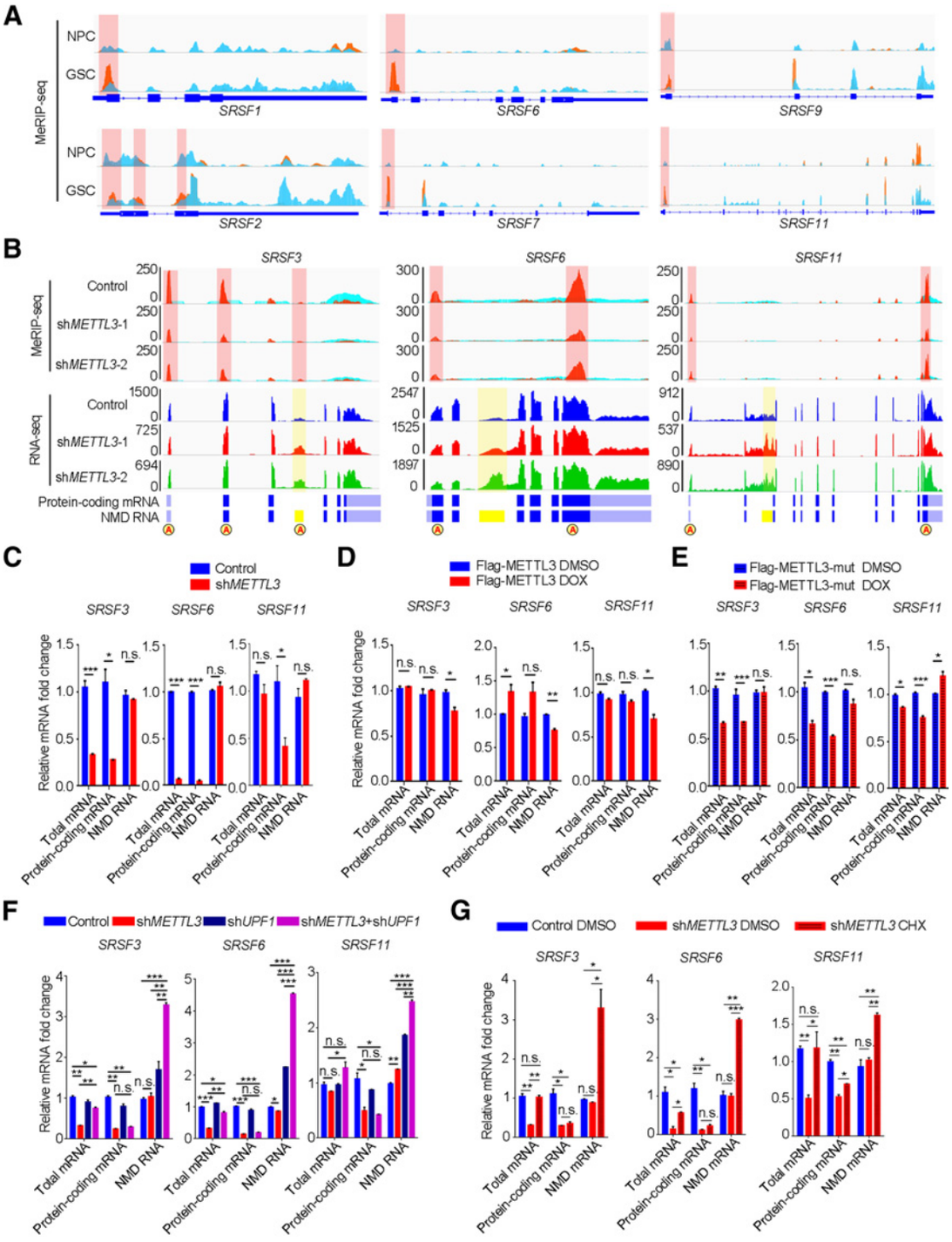

Figure 5.

METTL3-mediated NMD of *SRSFs* mRNAs rely on its m^{6}A methyltransferase activity. **A,** Genomic visualization of the m^{6}A immunoprecipitation–normalized signal in NPCs and GSCs of the *SRSFs*. The *x*-axis represents the genomic position. The *y*-axis shows normalized reads per million (rpm). **B,** Integrative Genomics Viewer plots of m^{6}A peaks and RNA-seq peaks at *SRSFs* mRNAs. The *y*-axis shows the sequence read number, blue boxes represent protein-coding exons, and yellow boxes represent NMD exons. RT-qPCR analysis of the total, protein-coding, or NMD RNA levels of *SRSFs* in U87MG cells transduced with sh*METTL3* (**C**) or METTL3 (**D**). **E,** RT-qPCR analysis of the total, protein-coding, or NMD RNA levels of *SRSFs* in U87MG cells transduced with a mutated catalytic domain (METTL3-mut). **F,** RT-qPCR analysis of the total, protein coding, or NMD RNA levels of *SRSFs* in U87MG cells treated with indicated shRNA(s). **G,** RT-qPCR analysis of the total, protein coding, or NMD RNA levels of *SRSF3, SRSF6*, and *SRSF11* in *METTL3*-KD U87MG cells treated with with 10 μg/mL cycloheximide (CHX) or DMSO during an 8 hour time course. *, $P < 0.05$; **, $P < 0.01$; ***, $P < 0.001$ is based on Student *t* test. Values are mean ± SD of three independent experiments. n.s., no significant difference.

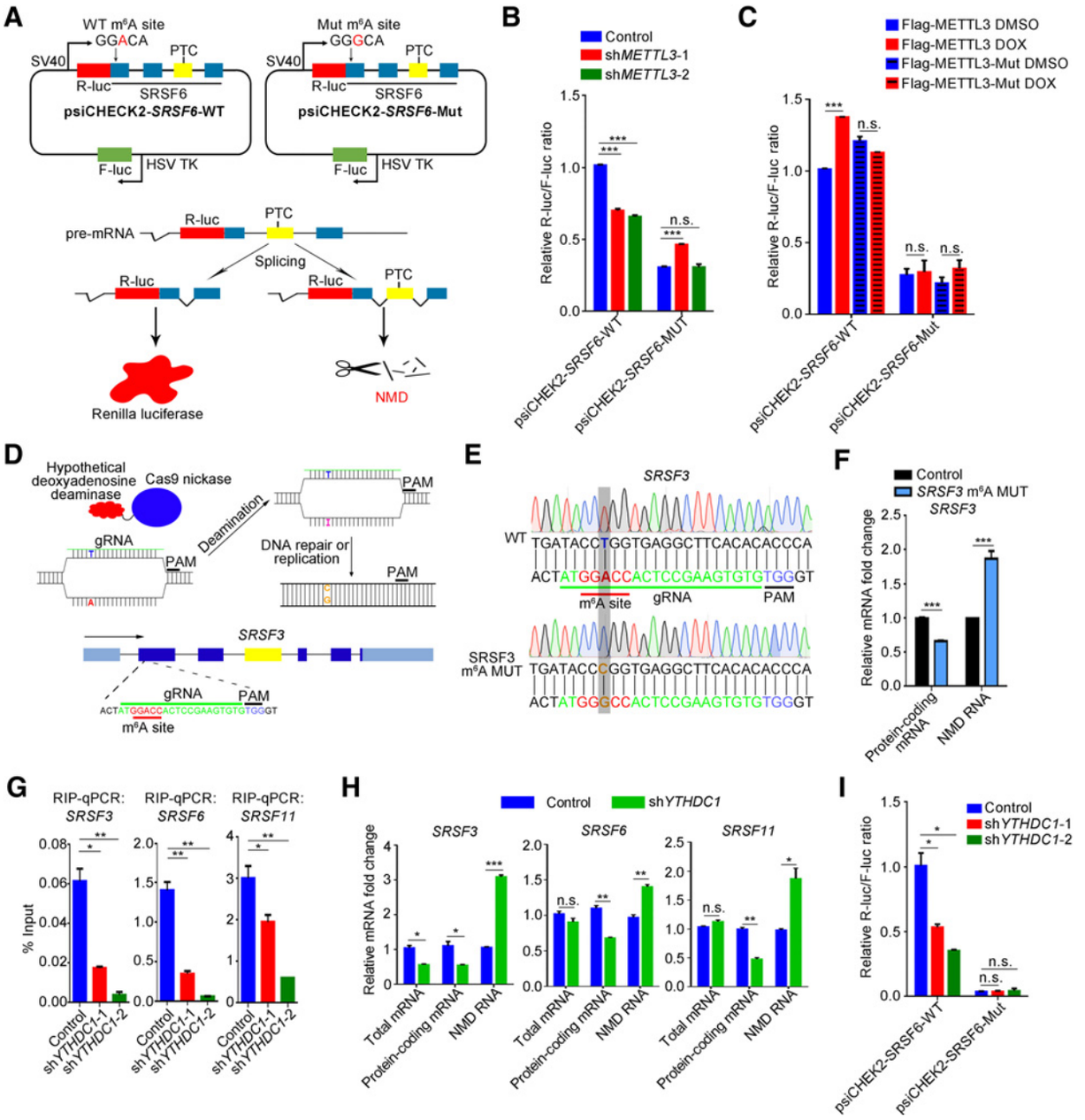

Figure 6.

The m^{6}A modification around start codon of splicing factors modulates NMD through YTHDC1. **A,** Schematic illustration of WT *SRSF6* minigene or m^{6}A consensus sequence mutant (A-to-G mutation) reporter constructs. *SRSF6* minigene was fused with *Renilla* luciferase reporter. NMD splicing of *SRSF6* minigene reporter cannot generate *Renilla* luciferase. F-luc, firefly luciferase; R-luc, *Renilla* luciferase. **B,** Relative luciferase activity of *SRSF6* minigene with wild-type or mutated m^{6}A sites after cotransfection with control shRNA, or *METTL3* shRNA in U87MG cells. *Renilla* luciferase activity was measured and normalized to firefly luciferase activity. **C,** Relative luciferase activity of *SRSF6* minigene with wild-type or mutated m^{6}A sites after cotransfection with WT METTL3 or METTL3-mut in U87MG cells. **D,** Schematic illustration of base editing system. **E,** Sequence of *SRSF3* in WT and m^{6}A site-edited U87MG cells. **F,** RT-qPCR analysis of the total or NMD RNA levels of *SRSF3* in WT and m^{6}A site-edited U87MG cells. **G,** RIP-qPCR analysis of YTHDC1 in U87MG cells and negative control cells (*YTHDC1*-KD U87MG cells). **H,** RT-qPCR analysis of the total, protein-coding, or NMD RNA levels of *SRSFs* in U87MG cells transduced with sh*YTHDC1*. **I,** Relative luciferase activity of *SRSF6* minigene with wild-type or mutated m^{6}A sites or *SRSF3* minigene after cotransfection with control shRNA, or *YTHDC1* shRNA in U87MG cells. *, $P < 0.05$; **, $P < 0.01$; ***, $P < 0.001$ is based on Student *t* test. Values are mean ± SD of three independent experiments. n.s., no significant difference.

GSE74397 (7) and GSE58352 (2), we found that YTHDC1 binds near the start codon region of *SRSFs* mRNAs (Supplementary Fig. S7J). KD *YTHDC1* led to the accumulation of NMD of *SRSF3*, *SRSF6*, and *SRSF11* mRNAs in GBM cells (Fig. 6H). Moreover, KD *YTHDC1* could affect the luciferase activity of the WT *SRSF6* minigene reporter but not the *SRSF6* reporter with the mutated

m^{6}A site (Fig. 6I). Together, these data suggest that *YTHDC1* KD-mediated NMD is dependent on m^{6}A around start codon of the mRNA in GBM cells.

KD of the m^{6}A methyltransferase *METTL3* results in dysregulation of alternative splicing events in GBM

We compared the alterative splicing events in *METTL3* KD U87MG cells compared with U87MG control cells. Using the rMATS tool, a total number of alternative splicing events was identified with an obvious change of exon inclusion levels (ψ, $\psi \geq 0.1$). We found that downregulation of splicing factors can affect various types of alternative splicing, including skipped exon (SE), alternative 5′ ss exon (A5SS), alternative 3′ ss exon (A3SS), retained intron (RI), and mutually exclusive exons (MXE), and, in particular, SE events in sh*METTL3* U87MG cells were most affected (Fig. 7A). Subsequent analysis indicated that the SE type of alternative splicing was negatively regulated by *METTL3*-KD, whereas A3SS, MXE, and RI were positively regulated by *METTL3*-KD (estimated by changes of ψ after *METTL3*-KD; Fig. 7B). Next, we compared genes that were differentially spliced in *METTL3*-KD U87MG cells to cells with scrambled control shRNA. When analyzing the cellular functions of METTL3-regulated alternative events using GO, we found that METTL3 affected alternative splicing of a number of genes, such as *BCL-X* and *NCOR2*, with functions in cancer cell death and motility (Fig. 7C; Supplementary Fig. S8A).

BCL-X is a well-known example of genes critical for cancer that has splicing variants that can function as cancer biomarkers and therapeutic targets. The *BCL-XL* isoform is antiapoptotic in various cancer types, whereas the *BCL-XS* isoform is proapoptotic in cancer. Using semiquantitative RT-PCR and qPCR, we confirmed that KD of *METTL3* significantly shifted the transcription of *BCL-XL* into *BCL-XS* (Fig. 7D and E; Supplementary Fig. S8B). The protein levels of *BCL-XL* were also reduced in *METTL3*-KD GBM cells (Supplementary Fig. S8C). To examine whether the splicing alteration of *BCL-X* was responsible for the *METTL3*-KD phenotypes, we designed shRNAs to specifically target *BCL-XS* to inhibit the expression of *BCL-XS* but not *BCL-XL* (Supplementary Fig. S8D). As shown in Fig. 7F and G, *METTL3* and *BCL-XS* double-KD GBM cells grew significantly faster with reduced apoptosis than cells with the *METTL3*-KD alone. This phenotypic rescue suggests that *METTL3* maintains the tumorigenicity of GBM cells, at least partially, through the splicing of *BCL-X*.

NCOR2 (also known as *SMRT*) exists in two major splicing isoforms, α and τ, which have different roles in preserving cellular identity and tissue homeostasis. Little is known about potential functional differences between these two isoforms in GBM. Using semiquantitative RT-PCR and qPCR, we revealed that KD of *METTL3* significantly increased the transcription of isoform α of *NCOR2* (Fig. 7H and I; Supplementary Fig. S8E). RT-PCR analysis showed that shRNAs targeting isoform α specifically inhibited its expression but not the τ isoform of *NCOR2* in U87MG cells (Supplementary Fig. S8F). Furthermore, we demonstrated that KD of the *NCOR2*α isoform partially rescued *METTL3* KD-induced inhibition of U87MG cell growth (Fig. 7J). In addition, our neurosphere formation data show that KD of the *NCOR2*α isoform significantly increased the neurosphere formation capacity and stem cell frequency in *METTL3*-KD U87MG cells (Fig. 7K and L), and together these data suggest that the NCOR2α isoform may play an important role in the regulation of GSC self-renewal.

Discussion

In this study, we established a novel mechanism for m^{6}A modifications around start codon of mRNA splicing factors in modulating NMD of these splicing factors. In addition, we found that METTL3 modulated alternative splicing of *BCLX* and *NCOR2*, which leads to GBM tumor outgrowth and self-renewal. Unlike previous studies, reporting that m^{6}A modifications at 3′-terminal ends are destabilizers of mRNA, our study revealed that m^{6}A modifications around start codon stabilize the mRNAs of *SRSFs* by preventing NMD. By preventing NMD and promoting mRNA degradation, m^{6}A modifications act as a molecular rheostat to finely adjust the transcript levels of *SRSFs* to influence alternative splicing events.

The role that METTL3 plays in cancer is complex. Two research teams reported opposite conclusions on the role that METTL3 plays in the self-renewal and tumorigenesis of GSCs. The reasons for these opposite conclusions may depend on the patients from whom the GBM cells originated and other compensatory genetic mutations and epigenetic changes in GBM cells. In this study, we chose clinical GBM samples from different stages, knocked down *METTL3* expression using both sgRNAs and shRNAs in primary GBM cells, and validated our findings using catalytic inactive mutants of METTL3. All of these results consistently demonstrated that METTL3 promotes proliferation and self-renewal of GBM cells. Notably, the oncogenic ability of METTL3 is dependent upon the m^{6}A methyltransferase catalytic domain. Interestingly, although KD *METTL14* expression reduced mRNA m^{6}A levels in GSCs (22), KO of *METTL14* has no effect on GBM oncogenicity. A recent study in AML cells showed that METTL3 bound the promoter regions of active genes (about 80 genes) independent of METTL14 (33). They also showed that CEBPZ is required for recruitment of METTL3 to the promoters. Their results indicate that specialized partner proteins might exist at splicing factor loci in GBM cells that give clues to decipher METTL14-independent METTL3's functions in GBM.

M^{6}A modifications may play different roles at different developmental stages of GMB tumors. In glioma, the mutation of isocitrate dehydrogenase 1 (*IDH1*) occurs frequently, which results in accumulation of the metabolic by-product 2-hydroxyglutarate (2-HG). The 2-HG could inhibit FTO activity, thereby increasing global m^{6}A modifications and contributing to cancer initiation. In the late stage of glioma, high m^{6}A modification levels may increase epigenetic reprogramming of non-GSCs into GSCs, whereas KD *METTL3* may reduce the proportion of GSCs in GBM. This hypothesis was indirectly verified by the observation that KD of *METTL3* in pluripotent stem cells, at naïve or primed states, resulted in different cell fate transitions (34). Thus, strategies designed to reduce levels of m^{6}A modifications may provide a means to target malignant GBM and to develop more effective therapies.

The prevailing goal of understanding the regulatory roles of m^{6}A modifications in RNA processing has been mainly focused on the regulation of mRNA translation or mRNA stability. Indeed, we found that METTL3 regulates the stability of a specific set of transcripts, such as apoptosis pathways and glial differentiation genes, in GBM. The m^{6}A-binding protein YTHDF2 may recognize these methylated mRNAs, leading to their decay and subsequently to decreased cell apoptosis and differentiation, thereby promoting GBM tumor growth and dedifferentiation. Another m^{6}A modification reader, YTHDC1, is involved in the process of

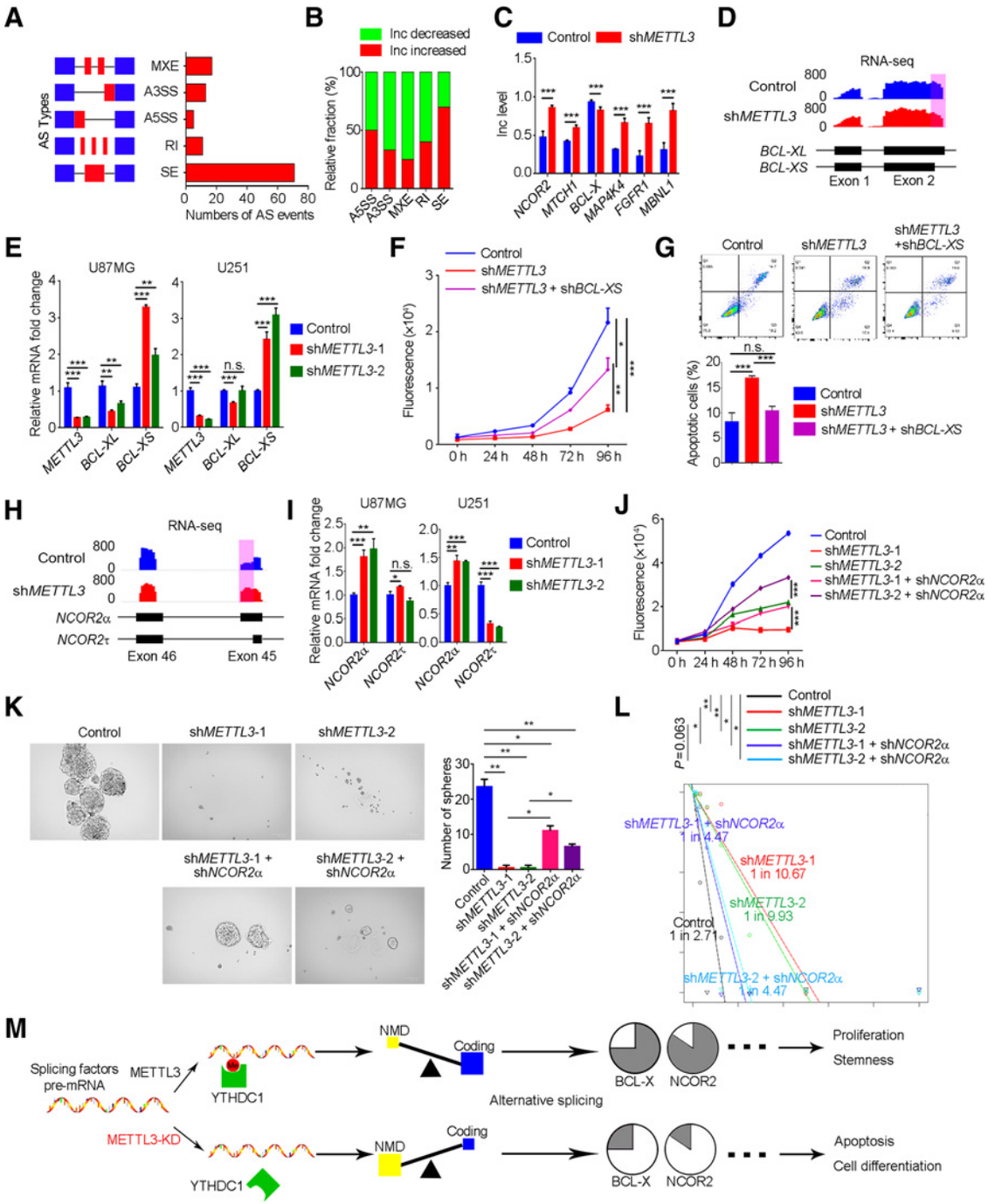

Figure 7.

METTL3 regulates *BCL-X* and *NCOR2* alternative splicing in GBM cells. **A,** The amount of changed alternative splicing events in U87MG cells transduced with sh*METTL3*. **B,** The relative fraction of each alternative splicing event affected either positively or negatively by METTL3. **C,** Representative genes with significantly changed alternative splicing events. **D,** Integrative Genomics Viewer plot illustrating the splicing changes of *BCL-X* promoted by METTL3. **E,** RT-qPCR analysis of splicing changes of *BCL-X* after *METTL3* KD. **F,** The cell viability tests of U87MG cells transduced with sh*METTL3* and/or sh*BCL-XS* were performed using CellTiter-Glo. **G,** The proportion of apoptotic cells in U87MG cells transduced with sh*METTL3* and/or sh*BCL-XS* was evaluated by flow cytometry. **H,** Integrative Genomics Viewer plot illustrating the splicing changes of *NCOR2* promoted by METTL3. **I,** RT-qPCR analysis of splicing changes of *NCOR2* after *METTL3* KD. **J,** The cell viability tests of U87MG cells transduced with sh*METTL3* and/or sh*NCOR2* were performed using CellTiter-Glo. **K,** U87MG cells were transduced with sh*METTL3* and/or sh*NCOR2*. The number of spheres formed was counted after transferring to stem cell culture condition for 7 days. **L,** Limiting dilution assay of GSCs transduced with sh*METTL3* and/or sh*NCOR2*. **M,** Schematic illustration of the working model. *, $P < 0.05$; **, $P < 0.01$; ***, $P < 0.001$ is based on Student *t* test. Values are mean ± SD of three independent experiments. n.s., no significant difference.

alternative splicing through recruitment and modulation of splicing factors to their targeted RNAs (35). We have presented a number of findings supporting the notion that m^{6}A modifications modulate the NMD of splicing factors. The NMD pathway protects eukaryotic cells by reducing the production of harmful truncated proteins translated from PTC-bearing mRNA transcripts. In our study, the reduced m^{6}A modifications by KD *METTL3* consequently led to the degradation of *SRSFs* transcripts via triggering NMD and thus control of GBM initiation and progression. It should be noted that KD *METTL3* affected not only YTHDC1-mediated NMD but also the m^{6}A-mediated mRNA degradation. Therefore, the effect of KO *YTHDC1* on GBM phenotype was not as significant as that of KD/KO *METTL3*.

SRSFs proteins are known for their ability to promote exon inclusion and exon-skipping events, suggesting the regulatory role of SRSFs proteins in alternative events. Brain tissue has been found to have particularly high levels of alternative splicing (36, 37). Consistently, a large number of cancer-relevant genes have undergone splice alterations in GBM (38–40). The importance of alternative splicing in the development of GBM was further reinforced by the findings that a large number of splicing factors were overexpressed in GBM (41, 42), yet the mechanisms responsible for this upregulation and its clinical relevance remain to be fully addressed. Our results support a model where METTL3 controls the cancer-relevant phenotypes of GBM cells by promoting the expression of SRSFs. This subsequently results in the creation of cancer-specific alternative splicing patterns, such as the preferential expression of the antiapoptotic transcript variant of *BCL-X* and the GSC-promoting transcript variant of *NCOR2* (Fig. 7M). It is worth noting that analysis of clinical outcomes revealed significant relationships between combined expression of METTL3 and splicing factors with GBM patient prognosis.

Taken together, this study provides an important mechanistic insight into how m^{6}A methyltransferase METTL3 serves as an NMD regulator of splicing factors with potential clinical implications of alternative splicing events of *BCL-XS* and *NCOR2*. Our study also demonstrates that expression of METTL3 can be used to dissect the molecular differences between histologically similar GBM entities and to help predict GBM prognosis.

Disclosure of Potential Conflicts of Interest

No potential conflicts of interest were disclosed.

Authors' Contributions

Conception and design: F. Li, Y. Yi, Y. Miao, Q. Cao, W. Zhao
Development of methodology: F. Li, Y. Yi, Y. Miao, C. Zou, Y. Zheng, D. Chen, F. Zhi, Q. Cao, W. Zhao
Acquisition of data (provided animals, acquired and managed patients, provided facilities, etc.): Y. Miao, W. Long, C. Zou, K. Zhu, Q. Cao, W. Zhao
Analysis and interpretation of data (e.g., statistical analysis, biostatistics, computational analysis): F. Li, Y. Yi, Y. Miao, T. Long, Y. Zheng, X. Wu, J. Ding, Q. Cao, W. Zhao
Writing, review, and/or revision of the manuscript: F. Li, Y. Yi, Y. Miao, Q. Cao, W. Zhao
Administrative, technical, or material support (i.e., reporting or organizing data, constructing databases): F. Li, Y. Miao, W. Long, T. Long, S. Chen, W. Cheng, Q. Xu, J. Wang, Q. Liu, F. Zhi, J. Ren, Q. Cao, W. Zhao
Study supervision: Q. Cao, W. Zhao

Acknowledgments

This work was supported by National Natural Science Foundation of China (81572766, 81702784, 81972651, 31771630, 81802974, 31771462, 81772614, 31471252, 31500813, and 31871009), Guangdong Innovative and Entrepreneurial Research Team Program (2016ZT06S029), the Natural Science Foundation of Guangdong Province (2017A030312009, 2017A030310228, 2014TQ01R387, 2017A030313134, and 2016A030313238), the Special funds for Dapeng New District Industry Development (KY20160309), and Natural Science Foundation of Jiangsu Province (BK20181156). Q. Cao is supported by U.S. Department of Defense (W81XWH-15-1-0639 and W81XWH-17-1-0357), American Cancer Society (TBE-128382), and NIH/NCI (R01CA208257).

The costs of publication of this article were defrayed in part by the payment of page charges. This article must therefore be hereby marked *advertisement* in accordance with 18 U.S.C. Section 1734 solely to indicate this fact.

Received September 14, 2018; revised January 10, 2019; accepted September 11, 2019; published first September 17, 2019.

References

1. Desrosiers R, Friderici K, Rottman F. Identification of methylated nucleosides in messenger RNA from Novikoff hepatoma cells. Proc Natl Acad Sci U S A 1974;71:3971–5.
2. Dominissini D, Moshitch-Moshkovitz S, Schwartz S, Salmon-Divon M, Ungar L, Osenberg S, et al. Topology of the human and mouse m6A RNA methylomes revealed by m6A-seq. Nature 2012;485:201–6.
3. Meyer KD, Saletore Y, Zumbo P, Elemento O, Mason CE, Jaffrey SR. Comprehensive analysis of mRNA methylation reveals enrichment in 3′ UTRs and near stop codons. Cell 2012;149:1635–46.
4. Zhao X, Yang Y, Sun BF, Shi Y, Yang X, Xiao W, et al. FTO-dependent demethylation of N6-methyladenosine regulates mRNA splicing and is required for adipogenesis. Cell Res 2014;24:1403–19.
5. Bartosovic M, Molares HC, Gregorova P, Hrossova D, Kudla G, Vanacova S. N6-methyladenosine demethylase FTO targets pre-mRNAs and regulates alternative splicing and 3′-end processing. Nucleic Acids Res 2017;45:11356–70.
6. Fustin JM, Doi M, Yamaguchi Y, Hida H, Nishimura S, Yoshida M, et al. RNA-methylation-dependent RNA processing controls the speed of the circadian clock. Cell 2013;155:793–806.
7. Zheng G, Dahl JA, Niu Y, Fedorcsak P, Huang CM, Li CJ, et al. ALKBH5 is a mammalian RNA demethylase that impacts RNA metabolism and mouse fertility. Mol Cell 2013;49:18–29.
8. Meyer KD, Patil DP, Zhou J, Zinoviev A, Skabkin MA, Elemento O, et al. 5′ UTR m(6)A promotes cap-independent translation. Cell 2015;163:999–1010.
9. Wang X, Zhao BS, Roundtree IA, Lu Z, Han D, Ma H, et al. N(6)-methyladenosine modulates messenger RNA translation efficiency. Cell 2015;161:1388–99.
10. Wang X, Lu Z, Gomez A, Hon GC, Yue Y, Han D, et al. N6-methyladenosine-dependent regulation of messenger RNA stability. Nature 2014;505:117–20.
11. Wang Y, Li Y, Toth JI, Petroski MD, Zhang Z, Zhao JC. N6-methyladenosine modification destabilizes developmental regulators in embryonic stem cells. Nat Cell Biol 2014;16:191–8.
12. Jia G, Fu Y, Zhao X, Dai Q, Zheng G, Yang Y, et al. N6-methyladenosine in nuclear RNA is a major substrate of the obesity-associated FTO. Nat Chem Biol 2011;7:885–7.
13. Liu J, Yue Y, Han D, Wang X, Fu Y, Zhang L, et al. A METTL3-METTL14 complex mediates mammalian nuclear RNA N6-adenosine methylation. Nat Chem Biol 2014;10:93–5.
14. Shi H, Wang X, Lu Z, Zhao BS, Ma H, Hsu PJ, et al. YTHDF3 facilitates translation and decay of N(6)-methyladenosine-modified RNA. Cell Res 2017;27:315–28.
15. Xu C, Wang X, Liu K, Roundtree IA, Tempel W, Li Y, et al. Structural basis for selective binding of m6A RNA by the YTHDC1 YTH domain. Nat Chem Biol 2014;10:927–9.
16. Hsu PJ, Zhu Y, Ma H, Guo Y, Shi X, Liu Y, et al. Ythdc2 is an N(6)-methyladenosine binding protein that regulates mammalian spermatogenesis. Cell Res 2017;27:1115–27.

17. Lin S, Choe J, Du P, Triboulet R, Gregory RI. The m(6)A methyltransferase METTL3 promotes translation in human cancer cells. Mol Cell 2016;62: 335–45.
18. Chen M, Wei L, Law CT, Tsang FH, Shen J, Cheng CL, et al. RNA N6-methyladenosine methyltransferase-like 3 promotes liver cancer progression through YTHDF2-dependent posttranscriptional silencing of SOCS2. Hepatology 2018;67:2254–70.
19. Vu LP, Pickering BF, Cheng Y, Zaccara S, Nguyen D, Minuesa G, et al. The N(6)-methyladenosine (m(6)A)-forming enzyme METTL3 controls myeloid differentiation of normal hematopoietic and leukemia cells. Nat Med 2017;23:1369–76.
20. Li Z, Weng H, Su R, Weng X, Zuo Z, Li C, et al. FTO plays an oncogenic role in acute myeloid leukemia as a N(6)-methyladenosine RNA demethylase. Cancer Cell 2017;31:127–41.
21. Visvanathan A, Patil V, Arora A, Hegde AS, Arivazhagan A, Santosh V, et al. Essential role of METTL3-mediated m(6)A modification in glioma stem-like cells maintenance and radioresistance. Oncogene 2018;37:522–33.
22. Cui Q, Shi H, Ye P, Li L, Qu Q, Sun G, et al. m(6)A RNA methylation regulates the self-renewal and tumorigenesis of glioblastoma stem cells. Cell Rep 2017;18:2622–34.
23. Zhang S, Zhao BS, Zhou A, Lin K, Zheng S, Lu Z, et al. m^6A demethylase ALKBH5 maintains tumorigenicity of glioblastoma stem-like cells by sustaining FOXM1 expression and cell proliferation program. Cancer Cell 2017;31:591–606.
24. Ozawa T, James CD. Establishing intracranial brain tumor xenografts with subsequent analysis of tumor growth and response to therapy using bioluminescence imaging. J Vis Exp 2010. doi: 10.3791/1986.
25. Dominissini D, Moshitch-Moshkovitz S, Salmon-Divon M, Amariglio N, Rechavi G. Transcriptome-wide mapping of N(6)-methyladenosine by m (6)A-seq based on immunocapturing and massively parallel sequencing. Nat Protoc 2013;8:176–89.
26. Alcantara Llaguno S, Chen J, Kwon CH, Jackson EL, Li Y, Burns DK, et al. Malignant astrocytomas originate from neural stem/progenitor cells in a somatic tumor suppressor mouse model. Cancer Cell 2009;15:45–56.
27. Schwartz S, Mumbach MR, Jovanovic M, Wang T, Maciag K, Bushkin GG, et al. Perturbation of m6A writers reveals two distinct classes of mRNA methylation at internal and 5′ sites. Cell Rep 2014;8:284–96.
28. Murat A, Migliavacca E, Gorlia T, Lambiv WL, Shay T, Hamou MF, et al. Stem cell-related "self-renewal" signature and high epidermal growth factor receptor expression associated with resistance to concomitant chemoradiotherapy in glioblastoma. J Clin Oncol 2008;26:3015–24.
29. Kawaguchi A, Yajima N, Tsuchiya N, Homma J, Sano M, Natsumeda M, et al. Gene expression signature-based prognostic risk score in patients with glioblastoma. Cancer Sci 2013;104:1205–10.
30. Linder B, Grozhik AV, Olarerin-George AO, Meydan C, Mason CE, Jaffrey SR. Single-nucleotide-resolution mapping of m6A and m6Am throughout the transcriptome. Nat Methods 2015;12:767–72.
31. Jin S, Zhang X, Miao Y, Liang P, Zhu K, She Y, et al. m(6)A RNA modification controls autophagy through upregulating ULK1 protein abundance. Cell Res 2018;28:955–7.
32. Gaudelli NM, Komor AC, Rees HA, Packer MS, Badran AH, Bryson DI, et al. Programmable base editing of A*T to G*C in genomic DNA without DNA cleavage. Nature 2017;551:464–71.
33. Barbieri I, Tzelepis K, Pandolfini L, Shi J, Millan-Zambrano G, Robson SC, et al. Promoter-bound METTL3 maintains myeloid leukaemia by m(6)A-dependent translation control. Nature 2017;552:126–31.
34. Zhao BS, He C. Fate by RNA methylation: m6A steers stem cell pluripotency. Genome Biol 2015;16:43.
35. Xiao W, Adhikari S, Dahal U, Chen YS, Hao YJ, Sun BF, et al. Nuclear m(6)A reader YTHDC1 regulates mRNA splicing. Mol Cell 2016;61:507–19.
36. Yeo G, Holste D, Kreiman G, Burge CB. Variation in alternative splicing across human tissues. Genome Biol 2004;5:R74.
37. Modrek B, Resch A, Grasso C, Lee C. Genome-wide detection of alternative splicing in expressed sequences of human genes. Nucleic Acids Res 2001; 29:2850–9.
38. Cheung HC, Hai T, Zhu W, Baggerly KA, Tsavachidis S, Krahe R, et al. Splicing factors PTBP1 and PTBP2 promote proliferation and migration of glioma cell lines. Brain 2009;132:2277–88.
39. Lo HW, Zhu H, Cao X, Aldrich A, Ali-Osman F. A novel splice variant of GLI1 that promotes glioblastoma cell migration and invasion. Cancer Res 2009;69:6790–8.
40. Yu Y, Jiang X, Schoch BS, Carroll RS, Black PM, Johnson MD. Aberrant splicing of cyclin-dependent kinase-associated protein phosphatase KAP increases proliferation and migration in glioblastoma. Cancer Res 2007; 67:130–8.
41. Pavlyukov MS, Yu H, Bastola S, Minata M, Shender VO, Lee Y, et al. Apoptotic cell-derived extracellular vesicles promote malignancy of glioblastoma via intercellular transfer of splicing factors. Cancer Cell 2018;34: 119–35.
42. Lefave CV, Squatrito M, Vorlova S, Rocco GL, Brennan CW, Holland EC, et al. Splicing factor hnRNPH drives an oncogenic splicing switch in gliomas. EMBO J 2011;30:4084–97.